Electronic Supplementary Material (ESI) for Dalton Transactions.
This journal is © The Royal Society of Chemistry 2022

Electronic Supplementary Information

Facet and d-band center engineering of CuNi nanocrystals for efficient nitrate electroreduction to ammonia

Jiao Wang,[a] Linlin Zhang,[*a, b] Yuanyuan Wang,[a] Yongjian Niu,[a] Dong Fang,[a] Qingxiao Su,[a] and Cheng Wang [a]

[a] Institute for New Energy Materials and Low-Carbon Technologies

School of Material Science and Engineering

Tianjin Key Laboratory of Advanced Functional Porous Materials

Tianjin University of Technology

Tianjin 300384, People's Republic of China

[b] CAS Key Laboratory of Design and Assembly of Functional Nanostructures

Fujian Key Laboratory of Nanomaterials

Fujian Institute of Research on the Structure of Matter, Chinese Academy of Sciences

Fuzhou 350002, People's Republic of China

[*] Corresponding author: Linlin Zhang, zhanglinlin_cn@126.com

Table of contents

Table S1: Molar ratios of Cu/Ni in the bimetal catalysts obtained from the ICP-MS tests.

Table S2: Binding energies of different components in Cu 2p and Ni 2p XPS for the samples of $Cu_{0.5}$, $Ni_{0.5}$ and $Cu_{0.25}Ni_{0.25}$.

Table S3: Performance comparison with reported Cu or Ni-based catalysts for nitrate electroreduction to ammonia

Supplementary experimental details

Determination of NH_3/NH_4^+

Indophenol blue method. Firstly, both the pristine blank electrolyte and the cathodic electrolyte were diluted 200 folds with deionized water. Then, a series of standard solutions of NH_4Cl (0.4, 0.8, 1.2, 1.6, 2.0 ppm) in the diluted blank electrolyte were prepared to establish the standard curve. The strongest absorption peak appeared at 655 nm. Afterwards, 2 mL of the coloring solution (5 wt% $C_7H_6O_3$, 5 wt% $C_6H_5Na_3O_7 \cdot 2H_2O$ and 1 M NaOH), 1 mL of the oxidizing solution (NaClO (ρ = 4–4.9)) and 0.2 mL of the catalyst solution (1 wt% $C_5FeN_6Na_2O \cdot 2H_2O$) were added to 2 mL of the standard or diluted sample solutions in sequence. The mixtures were then kept undisturbed at room temperature for 2 h. UV-vis absorption spectra were recorded on a UV3900 spectrophotometer (Shimadzu) in the wavelength range from 500 to 800 nm at a scan rate of 300 nm min^{-1}. According to the standard curve and the measured absorbance, the concentration of ammonia produced from NO_3RR could be finally obtained.

^1H NMR spectra. A series of standard solutions of NH_4Cl (100, 200, 300, 400, 500 ppm) in the pristine blank electrolyte were prepared to establish the standard curve. The pH value of the standard solutions of NH_4Cl and the cathodic electrolyte were adjusted to 3.0 by the addition of 0.5 M H_2SO_4. The test solutions comprised of 0.5 mL of the above NH_4Cl solutions or cathodic electrolytes, 0.1 mL of DMSO (0.01 vol%) and 0.1 mL of D_2O aqueous solution. Then, 1H NMR spectra were acquired on a nuclear magnetic resonance spectrometer (AVANCE III HD 400 MHz, Bruker) after scanning 400 times in water suppression mode. Based on the standard curve and the measured peak area, the concentration of ammonia produced from NO_3RR could be obtained. To identify the origin of nitrogen in ammonia produced, isotope labelling experiments were carried out using $K^{15}NO_3$ to replace KNO_3 in the electrochemical tests and the corresponding products were analyzed using ^1H-NMR spectra in a similar way.

Determination of NO_2^- and NO_3^-

Ion chromatography (IC). Both the pristine blank electrolyte and the cathodic electrolytes were diluted 500 folds using deionized water. Standard solutions of NO_2^- (0.2, 0.4, 0.6, 0.8, 1.0 ppm) and NO_3^- (3, 6, 9, 12, 15 ppm) in diluted blank electrolyte were prepared to build the standard curves. The pH values of the standard solutions, diluted blank electrolyte and diluted cathodic electrolytes were adjusted to 7.0 using 0.5 M HCl. The concentrations of anions were measured using an anionic column (Metrosep A Supp 5-150/0.4) at room temperature with an eluent flow rate of 0.1 mL min^{-1}. The anionic eluent contained 3.2 mM Na_2CO_3 and 1.0 mM $NaHCO_3$. Termination of the retention time was set to 11 min and peaks assigned to NO_2^- and NO_3^- occurred at 6.35 and 9.5 min, respectively. According to the calibration curve and the measured peak areas, the concentrations of generated NO_2^- and remaining NO_3^- could be obtained.

Determination of N_2H_4

Watt-Chrisp method. Both the pristine blank electrolyte and the cathodic electrolyte were diluted 300 folds using deionized water. Standard solutions of N_2H_4 in the diluted blank electrolyte (0.2, 0.4, 0.6, 0.8, 1.0 ppm) were prepared to build the calibration curve. The color reagent was a mixture containing 0.5 g of p-dimethylaminobenzaldehyde, 25 mL of ethanol and 2.5 mL of concentrated HCl. Then, 0.1 mL of concentrated HCl solution was added to 4 mL of N_2H_4 standard solutions or diluted electrolytes to adjust the pH values of the solutions to the acidic range, followed by the addition of 0.5 mL of color reagent. The resulting solutions were then allowed to stand for 5 min. Subsequently, UV-vis absorption spectra were measured in the wavelength range of 400-500 nm at a scan rate of 300 nm min^{-1}. The maximum absorbance ought to occur at about 455 nm. According to the calibration curve and the measured absorbance, the concentration of N2H4 could be determined.

The equations involved in this work are listed as follows:

$\varepsilon_d = \int_{-\infty}^{n} n_d(\varepsilon)\varepsilon d\varepsilon / \int_{-\infty}^{n} n_d(\varepsilon) d\varepsilon$ **(1)**, where ε_d is the d-band center, ε is the energy relative to the fermi level and $n_d(\varepsilon)$ is the phtotoelectron intensity after the subtraction of the shirley-type background. The upper level of the integration was fixed at 8.0 eV for accurate comparison.

E (*vs*. RHE) = E (*vs*. Hg/HgO) + 0.059 × pH + 0.098 **(2)**, where E (*vs*. RHE) and E (*vs*. Hg/HgO) are the applied potentials relative to the reversible hydrogen electrode and to the Hg/HgO electrode, respectively.

$Y_{NH_3}=C(NH_3)\times V/(t\times m_{cat.})$ **(3),** $FE_{NH_3}=8F\times C(NH_3)\times V/(17Q)\times 100\%$ **(4)**, and $J_{NH_3} = (I\times FE_{NH_3})/A$ **(5)**, where Y_{NH_3}, FE_{NH_3} and J_{NH_3} are the yield, faradaic efficiency and partial current density of NH_3, respectively; $C(NH_3)$ is the molar concentration of measured NH_3, V is the volume of the electrolyte, t is the electrolysis time, $m_{cat.}$ is the mass of the loaded catalyst, F is the Faraday constant (96485 C mol^{-1}) and Q is the total charge passing through the electrode ($Q = \int_0^t j\,dt$, j is the geometric current density), I is the current during the constant potential electrolysis, A is the surface area of the cathode.

Selec. = $C(NH_3)/\Delta C(NO_3^-) \times 100\%$ **(6)**, where Selec. is the selectivity of NH_3, C_0 is the initial concentration of NO_3^- in the electrolyte and $\Delta C(NO_3^-)$ is the concentration difference of NO_3^- before and after electrolysis.

$EE_{NH_3} = (1.23-E_{NH3}^{0})FE_{NH_3}/(1.23-E)$ **(7)**, where EE_{NH_3} is the energy efficiency for nitrate electroreduction to ammonia, E_{NH3}^{0} is the equilibrium potential of nitrate electroreduction to ammonia (0.69 V), FE_{NH_3} is the faradaic efficiency for ammonia, 1.23 V is the equilibrium potential of water oxidation and E is the applied potential *vs*. RHE.

$Y_{NO_2^-} = C(NO_2^-)\times V/(t\times m_{cat.})$ **(8)**, $FE_{NO_2^-} = 2F\times C(NO_2^-)\times V/(46Q)\times 100\%$ **(9)**, where $Y_{NO_2^-}$ and $FE_{NO_2^-}$ are the yield and faradaic efficiency of NO_2^-, respectively; $C(NO_2^-)$ is the molar concentration of measured NO_2^-, V is the volume of the electrolyte, t is the electrolysis time, $m_{cat.}$ is the mass of the loaded catalyst, F is the Faraday constant (96485 C mol^{-1}) and Q is the total charge passing through the electrode ($Q = \int_0^t j\,dt$, j is the geometric current density).

$Y_{N_2H_4} = C(N_2H_4)\times V/(t\times m_{cat.})$ **(10)**, $FE_{N_2H_4} = 7F \times C(N_2H_4) \times V/(32Q) \times 100\%$ **(11)**, where $Y_{N_2H_4}$ and $FE_{N_2H_4}$ are the yield and faradaic efficiency of N_2H_4, respectively; $C(NO_2^-)$ is the molar concentration of measured NO_2^-, V is the volume of the electrolyte, t is the electrolysis time, $m_{cat.}$

is the mass of the loaded catalyst, F is the Faraday constant (96485 C mol^{-1}) and Q is the total charge passing through the electrode ($Q = \int_0^t j\,dt$, j is the geometric current density).

$E = a + b\log(|J_{NH_3}|)$ **(12)**, where E is the applied potential vs. RHE, J_{NH_3} is the partial current density of NH_3, a is a constant and b is the Tafel slope.

$\ln(C_0/C_t) = k_{ap}t$ **(13)**, where k_{ap} is the apparent rate constant, C_0 and C_t are the concentrations of NO_3^- in the electrolytes at the beginning and at reaction time t, respectively.

$1/r_0 = 1/(kK_{ads}C_0) + 1/k$ **(14)**, where K_{ads} is the equilibrium adsorption constants for NO_3^-, r_0 is the initial reduction rate of NO_3^- ($r_0 = k_{ap}C_0$), k is the rate constant for the adsorbed NO_3^-, C_0 is the initial concentration of NO_3^-.

$\Delta G_{ads} = -RT\ln K_{ads}$ **(15)**, whereΔGads is the adsorption free energy of NO_3^-, R is the gas constant, T is the reaction temperature and K_{ads} is the equilibrium adsorption constants for nitrate ions.

$i_k = Ae^{(-Ea/RT)}$ **(16)**, where Ea is the apparent activation energy, i_k is the kinetic current at -0.5 V, A is the pre-exponential factor, T is the reaction temperature and R is the universal gas constant.

$j_p = (-2.99\times10^5)n\alpha^{1/2}CD^{1/2}v^{1/2}$ **(17)**, where n is the charge transfer number, j_p is the peak current density(A cm^{-2}), α is transfer coefficient (0.5), C is the nitrate concentration in electrolytes (7.5×10^{-5} mol cm^{-3}), D is the diffusion coefficient of nitrate ions (2.0×10^{-5} cm^2 s^{-1}) and v is the scan rate (V s^{-1}).

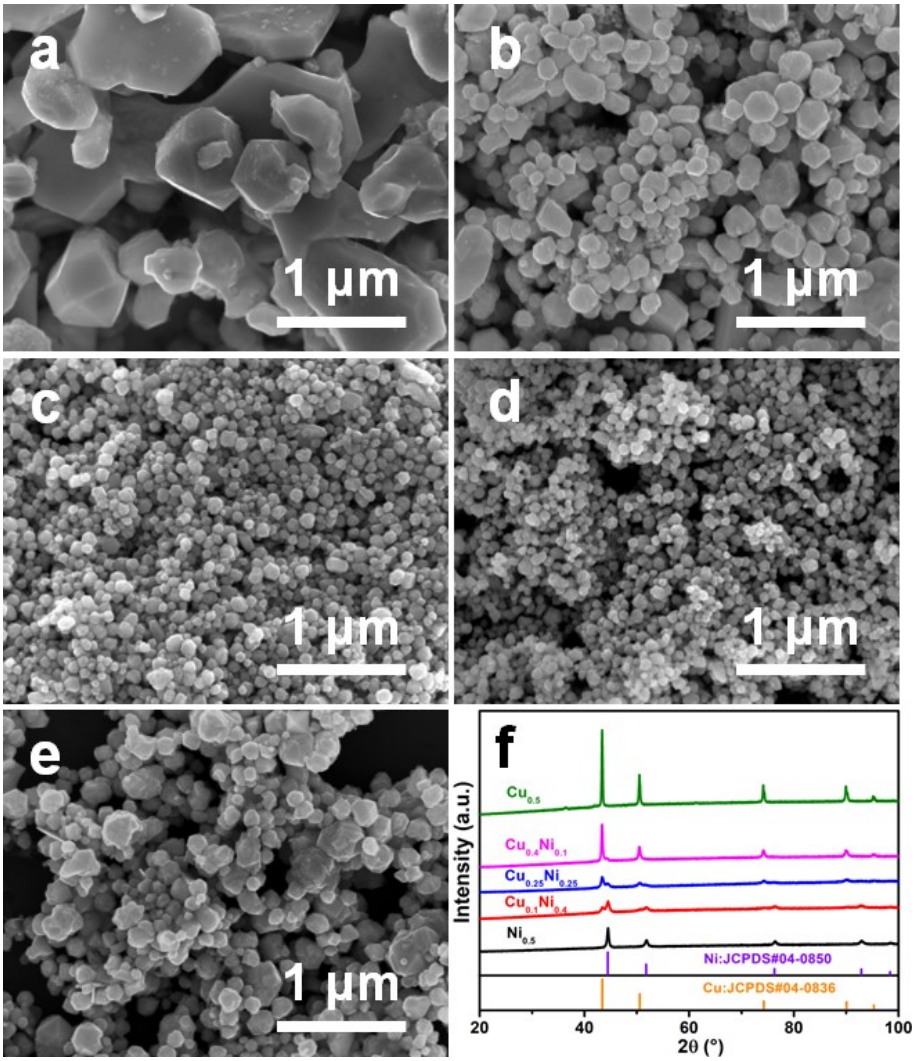

Figure S1. SEM images (a-e) and XRD patterns (f) for the samples of $Cu_{0.5}$ (a), $Cu_{0.4}Ni_{0.1}$ (b), $Cu_{0.25}Ni_{0.25}$ (c), $Cu_{0.1}Ni_{0.4}$ (d), and $Ni_{0.5}$ (e).

Table S1. Molar ratios of Cu/Ni in the bimetal catalysts obtained from the ICP-MS tests.

sample	$Cu_{0.1}Ni_{0.4}$	$Cu_{0.25}Ni_{0.25}$	$Cu_{0.4}Ni_{0.1}$
molar ratio of Cu/Ni	1/3.35	1/0.9	5.37/1

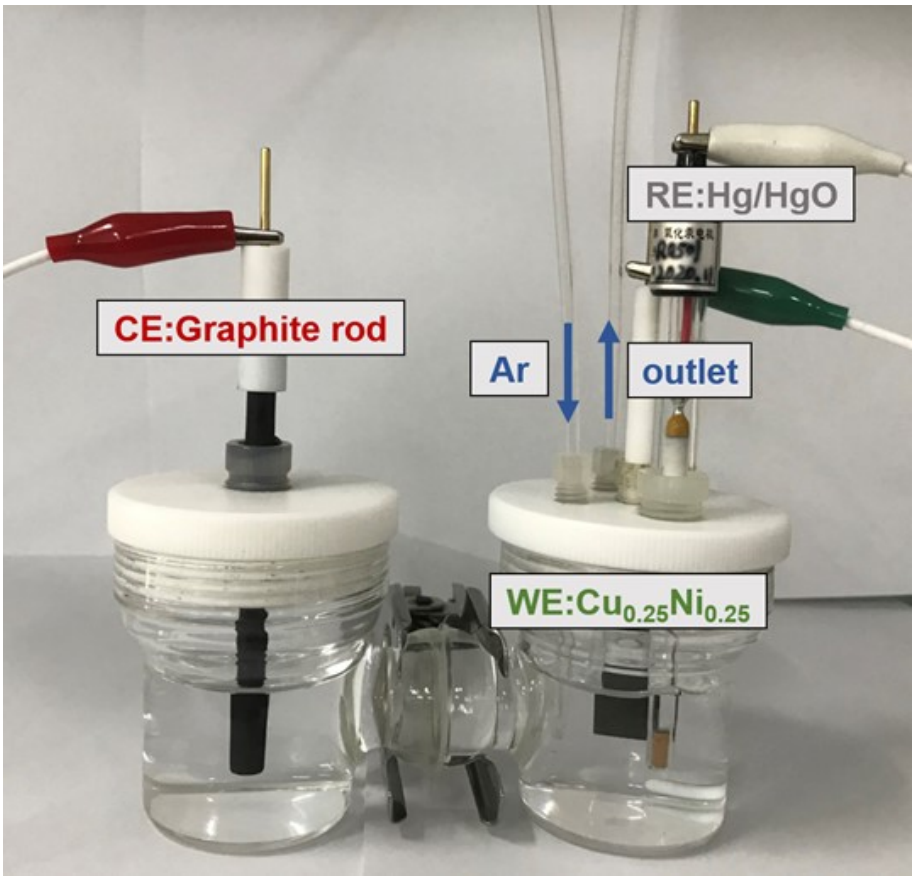

Figure S2. Photograph of the setup for NO_3RR.

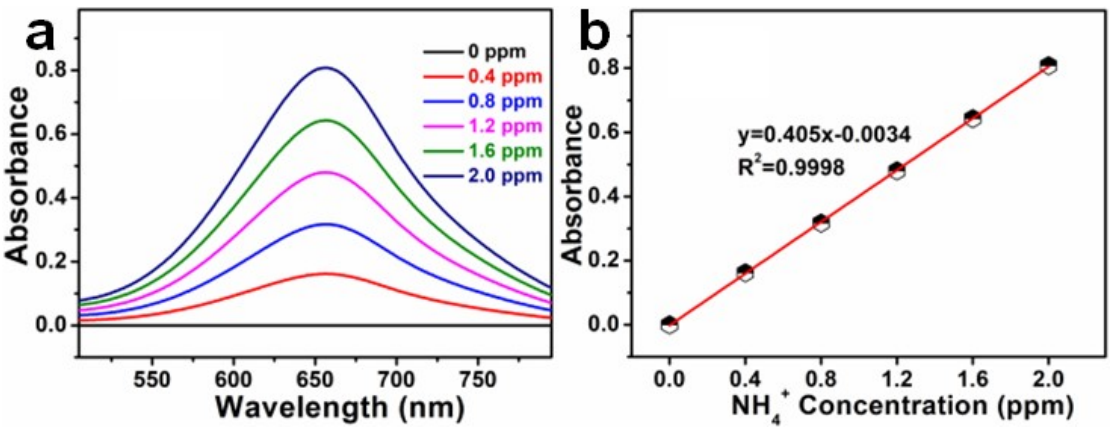

Figure S3. UV-vis absorption spectra of the standard NH_4Cl solutions stained with the indophenol

blue coloring agent (a) and the corresponding standard curve (b).

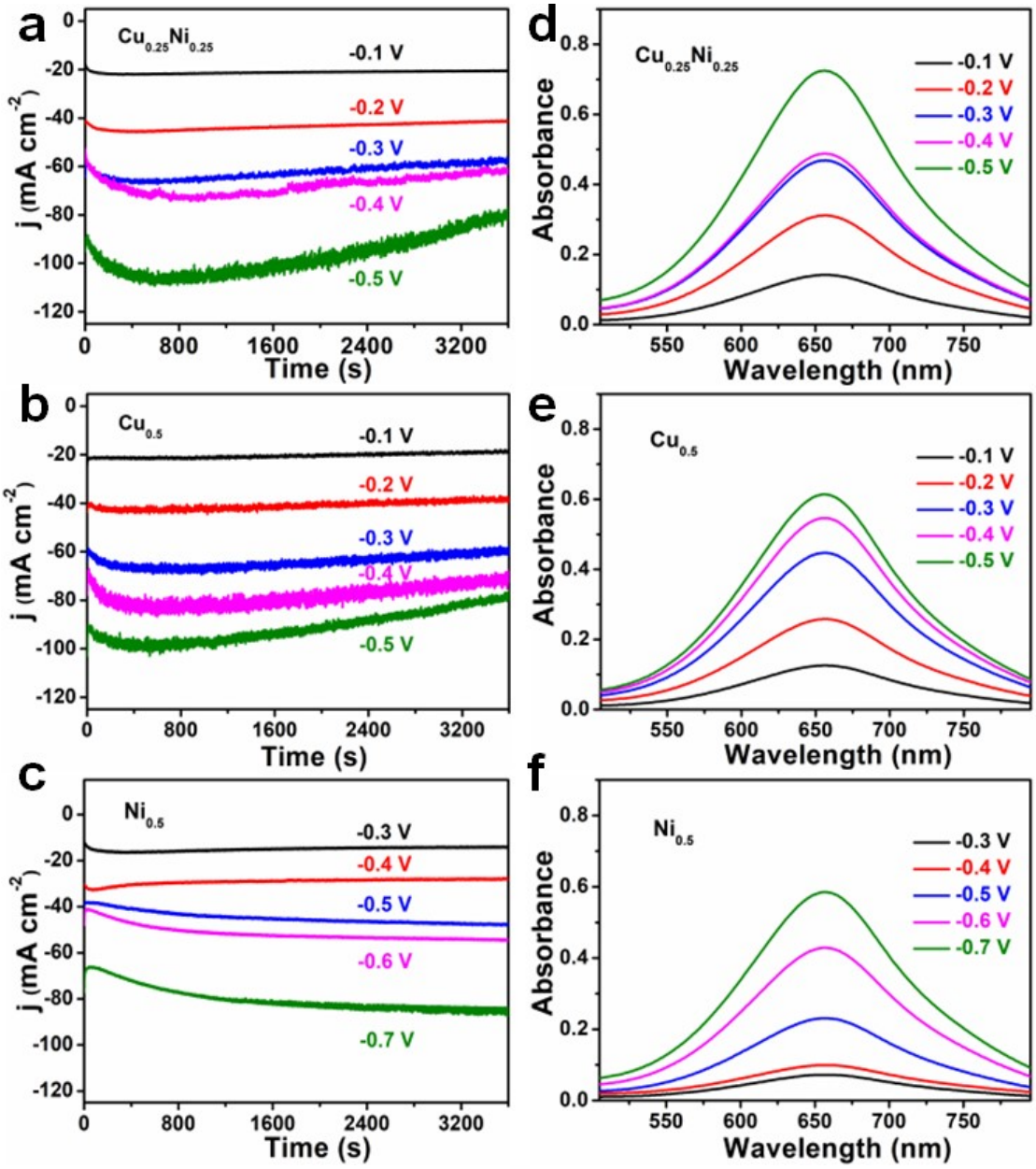

Figure S4. Chronoamperometric responses (a-c) and the corresponding UV-vis absorption spectra of the catholytes after electrolysis at different potentials stained with the indophenol blue (b-f) for the samples of $Cu_{0.25}Ni_{0.25}$ (a, c), $Cu_{0.5}$ (b, d) and $Ni_{0.5}$ (c, f).

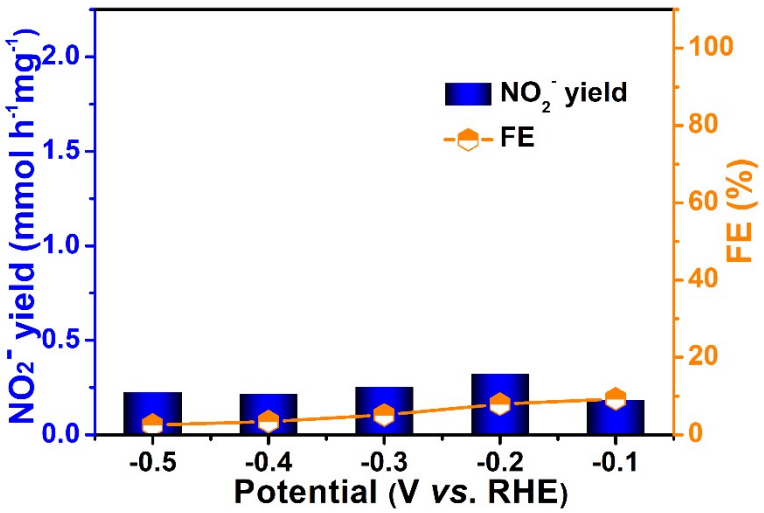

Figure S5. The yield and FE of the possible by-product of NO_2^- after electrolysis in 1 M KOH solutions containing 75 Mm KNO_3 at different potentials with $Cu_{0.25}Ni_{0.25}$ as the catalyst.

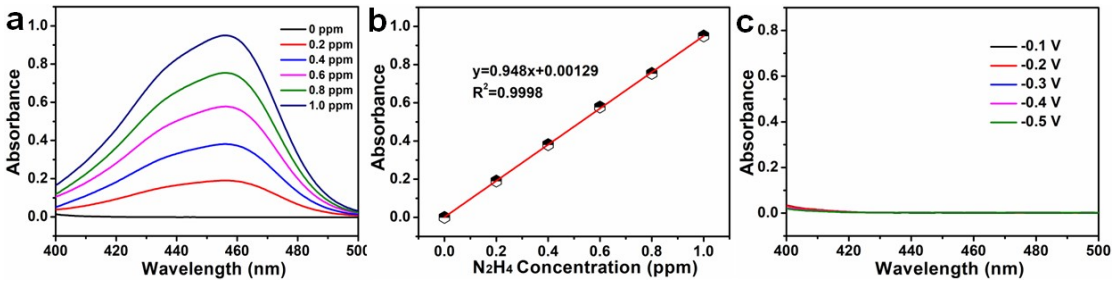

Figure S6. Determination of the possible by-product of N_2H_4 according to the Watt-Chrisp method. UV-vis absorption spectra of the standard solutions of N_2H_4 (a), the corresponding standard curve (b) and the UV-vis absorption spectra of the catholyte after electrolysis at different potentials with $Cu_{0.25}Ni_{0.25}$ as the catalyst (c).

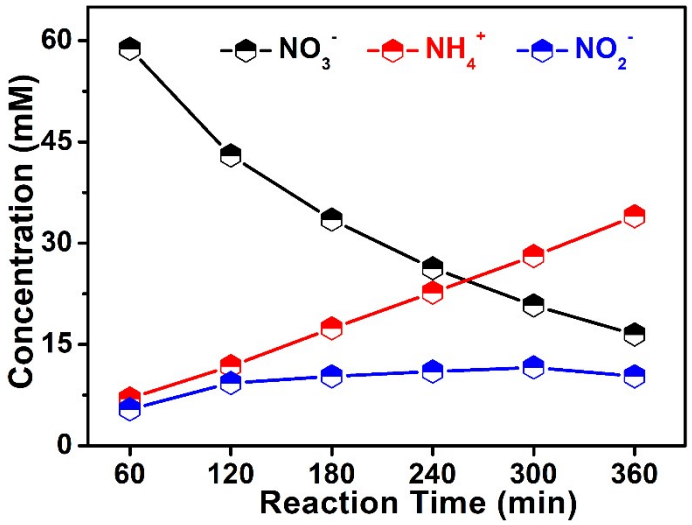

Figure S7. The concentration of NO_3^-, NO_2^- and NH_4^+ as a function of reaction time with $Cu_{0.25}Ni_{0.25}$ as the catalyst.

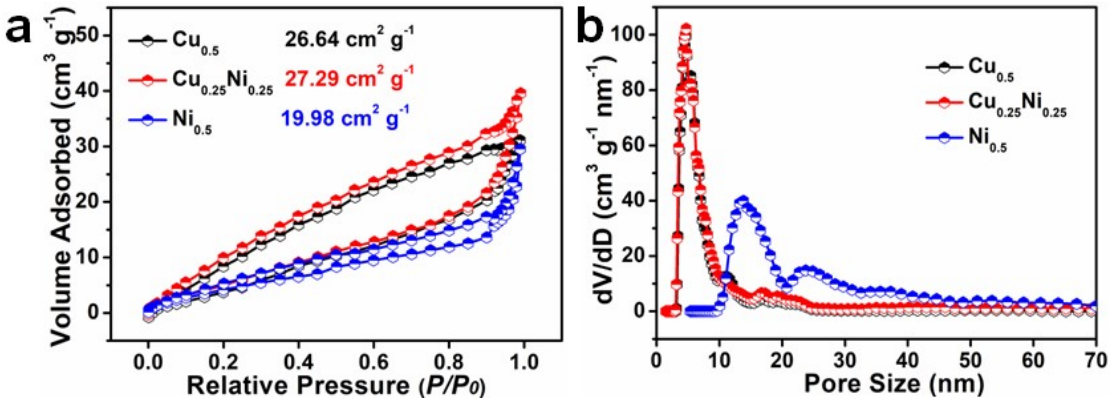

Figure S8. N_2 adsorption-desorption isotherms (a) and the corresponding pore size distributions (b) for the samples of $Cu_{0.25}Ni_{0.25}$, $Cu_{0.5}$ and $Ni_{0.5}$.

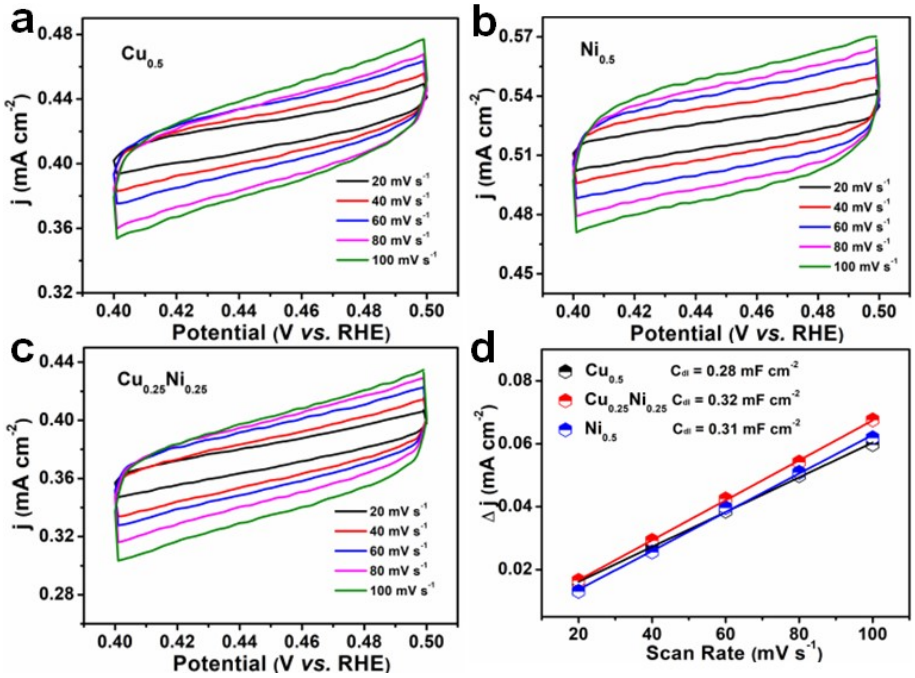

Figure S9. CV curves obtained at different scan rates in the non-faradaic potential ranges for the samples of$Cu_{0.5}$ (a), $Ni_{0.5}$ (b) and $Cu_{0.25}Ni_{0.25}$ (c) and the corresponding double layer capacitances (C_{dl}) (d).

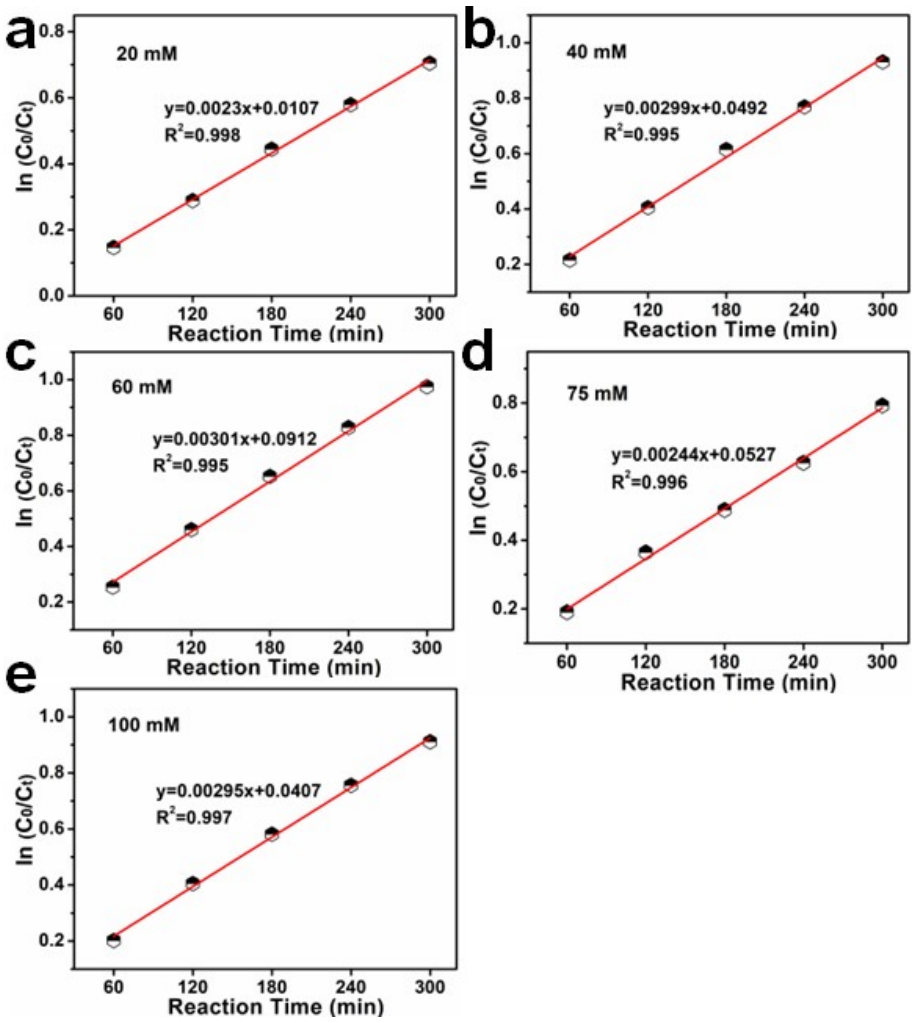

Figure S10. Linear fitting plots of $\ln C_0/C_t$ against the reaction time t according to the pseudo first order kinetic equation for $Cu_{0.5}$ with different initial nitrate concentrations in the electrolytes. (a) 20 mM, (b) 40 mM, (c) 60 mM, (d) 75 mM, (e) 100 mM.

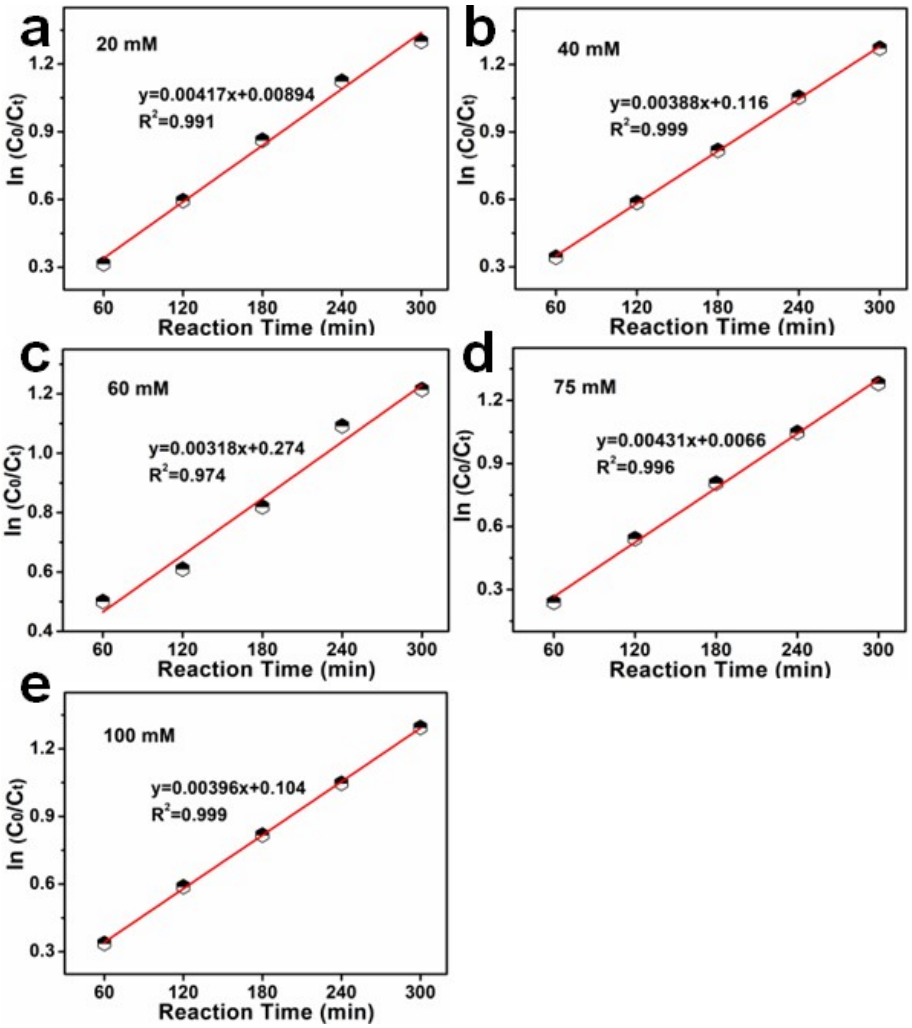

Figure S11. Linear fitting plots of $\ln C_0/C_t$ against the reaction time t according to the pseudo first order kinetic equation for $Cu_{0.25}Ni_{0.25}$ with different initial nitrate concentrations in the electrolytes. (a) 20 mM, (b) 40 mM, (c) 60 mM, (d) 75 mM, (e) 100 mM.

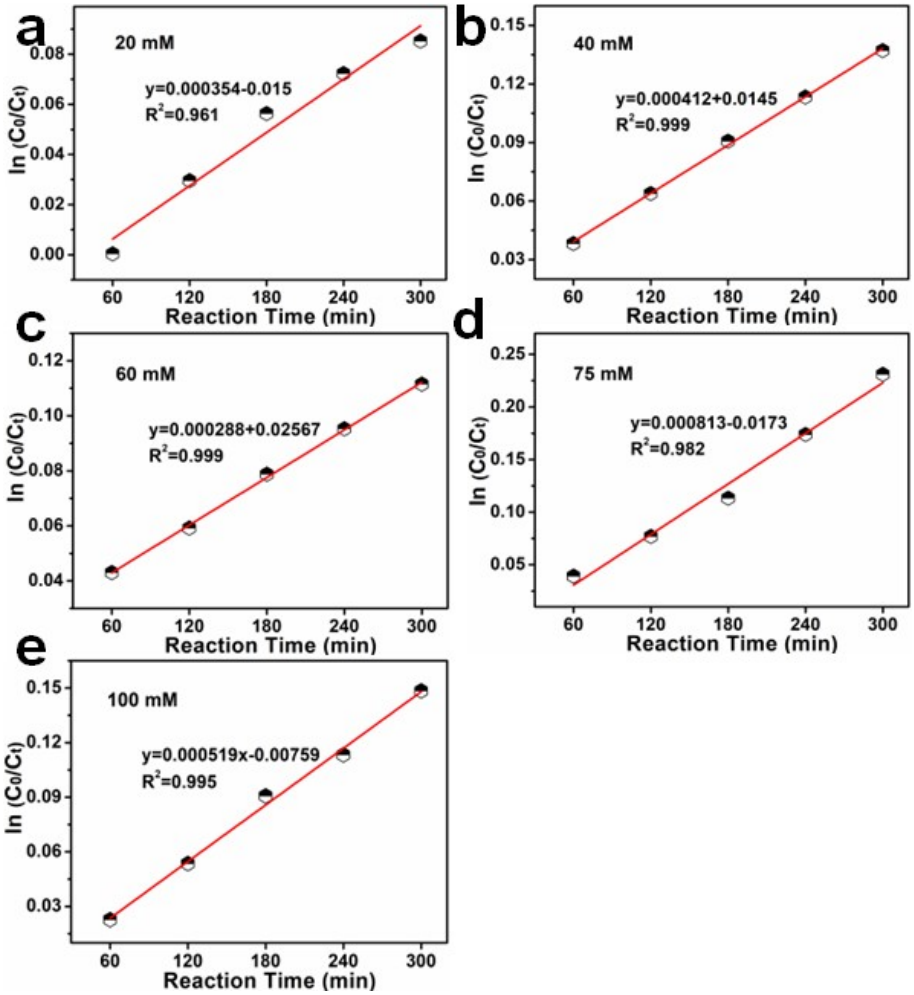

Figure S12. Linear fitting plots of $\ln C_0/C_t$ against the reaction time t according to the pseudo first order kinetic equation for $Ni_{0.5}$ with different initial nitrate concentrations in the electrolytes. (a) 20 mM, (b) 40 mM, (c) 60 mM, (d) 75 mM, (e) 100 mM.

Table S2. Binding energies of different components in Cu 2p and Ni 2p XPS for the samples of $Cu_{0.5}$, $Ni_{0.5}$ and $Cu_{0.25}Ni_{0.25}$.

Sample	Cu 2p				
	Cu 2p 3/2		Cu 2p 1/2		Sat. (eV)
	Cu^0/Cu^+ (eV)	Cu^{2+} (eV)	Cu^0/Cu^+ (eV)	Cu^{2+} (eV)	
$Cu_{0.5}$	932.48	952.32	934.52	954.31	941.66/943.83/962.5
$Cu_{0.25}Ni_{i0.25}$	932.33	952.29	933.86	953.82	
Sample	**Ni 2p**				
	Ni 2p 3/2		Ni 2p 1/2		Sat. (eV)
	Ni^0 (eV)	Ni^{2+} (eV)	Ni^0 (eV)	Ni^{2+} (eV)	
$Ni_{0.5}$	852.21	855.26	869.44	872.93	860.73/879.61
$Cu_{0.25}Ni_{0.25}$	852.66	855.66	869.97	873.45	861.02/879.17

Table S3. Performance comparison with reported Cu or Ni-based catalysts for nitrate electroreduction to ammonia

Catalyst	Potential	FE (%)	Selectivity (%)	Yield (mmol h^{-1} cm^{-2})	Ref.
$Cu_{0.25}Ni_{0.25}$	**-0.30** [a]	**94.5**	**65.0**	**0.5496**	**This wok**
Cu/Rgo/GP	-1.40 [b]	96.8	19.4	0.0145	[1]
CF@Cu_2O	-0.60 [a]	94.2	-	0.4418	[2]
pCuO-10	-0.50 [a]	89.0	-	0.2000	[3]
Cu-NBs-110	-0.15 [a]	95.0	95.3	1.3000	[4]
Cu/Cu-Mn_3O_4	-1.30 [a]	92.4	87.6	0.2100	[5]
Cu/Cu_2O NWs	-0.85 [a]	95.8	81.2	0.2449	[6]
Cu-N-C-800	-1.30 [b]	-	80.5	0.0003	[7]
$Cu_{49}Fe_1$	-0.70 [a]	94.5	86.8	0.2300	[8]
$Pd_{0.4}Cu_{0.6}$	-0.30 [a]	-	49.0	0.0002	[9]
Cu-Bi	-1.60 [b]	-	19.0	0.0053	[10]
Bi_2O_3/CC	-10.0 [c]	47.8	80.3	0.0027	[11]
TiO_{2-X}	-1.60 [b]	85.0	87.1	0.0225	[12]
Co/CoO NAs	-1.30 [b]	93.8	91.2	0.1940	[13]
nZVI@OMC-400	-1.30 [b]	60.1	39.5	0.0010	[14]
Fe SAC	-0.66 [a]	75.0	69.0	0.4600	[15]
Fe/Cu Composite	25.0 [c]	-	70.0	0.0600	[16]
Co_3O_4	-0.65 [a]	1.23	33.6	0.8540	[17]
FeNC/MC	-1.30 [b]	-	19.0	0.0005	[18]
$Sn_{0.8}Pd_{0.2}$/SS	-40.0 [c]	-	14.0	0.0013	[19]
Co_3O_4-TiO_2/Ti	-10.0 [c]	-	24.0	0.0008	[20]
Ni-NSA-V_{Ni}	-1.20 [b]	88.9	77.2	0.2360	[21]
Cu	-0.376 [a]	-	85	0.2714	[22]
Pd-Cu/γAl_2O_3	-0.844 [a]	-	19.6	0.0091	[23]
Pd/TiO_2	-0.70 [a]	92.05	-	0.0659	[24]
Ru-ST-12	-0.20 [a]	100	99.0	1.1700	[25]
Ni-Fe^0@ Fe_3O_4	5.0 [c]	-	10.4	0.0009	[26]

[a] The potentials were relative to the reversible hydrogen electrode (RHE).

[b] The potentials were relative to the saturated calomel electrode (SCE).

[c] The numbers were current densities (mA cm^{-2}) at which the constant current electrolysis were performed and the performances were assessed.

References

[1] D. Yin, Y. Liu, P. Song, P. Chen, X. Liu, L. Cai and L. Zhang, *Electrochimica Acta*., 2019, 324, 134846.

[2] Q.Y. Chen, X.G. An, Q. Liu, X. Q. Wu, L. S. Xie, J. Zhang, W. T. Yao, Mohamed S. Hamdy, Q. Q. Kong and X. P. Sun. *Chem. Commun*., 2022, 58, 517-520.

[3] Rahman Daiyan, Thanh Tran-Phu, Priyank Kumar,a Kevin Iputera, Zizheng Tong, Joshua Leverett, Muhammad Haider Ali Khan, Ali Asghar Esmailpour, Ali Jalili, Maggie Lim, Antonio Tricoli, Ru-Shi Liu, Xunyu Lu, Emma Lovell and Rose Ama. *Energy Environ. Sci*., 2021, 14, 3588-3598.

[4] Q. Hu, Y. J. Qin, X. D. Wang, Z. Y. Wang, X. W. Huang, H. J. Zheng, Keru Gao, Hengpan Yang, P. X. Zhang, M. H. Shao and C. X. He. *Energy Environ. Sci*., 2021, 14, 4989-4997.

[5] H. J. Wang, Q. Q. Mao, T. L. Ren, T. Q. Zhou, K. Deng, Z. Q. Wang, X. N. Li, Y. Xu, and L. Wang. ACS Appl. Mater. Interfaces., 2021, 13, 37, 44733-44741.

[6] Y. Wang, W. Zhou, R. Jia, Y. Yu and B. Zhang, Angew. Chem. Int. Ed., 2020, 59, 5350-5354.

[7] Tonghe Zhu, Qiongshan Chen, Peng Liao, Weijian Duan, Sheng Liang, Zhang Yan, and Chunhua Feng. *Small*.,2020, 16, 2004526.

[8] C. Wang, Z. Liu, T. Hu, J. Li, L. Dong, F. Du, C. Li and C. Guo, *ChemSusChem*, 2021, 14, 1825-1829.

[9] J. F. Su, I. Ruzybayev, I. Shah and C. P. Huang, Appl. Catal. B: Environ., 2016, 180, 199-209.

[10] Weichun Gao, Lulu Gao, Dan Li, Kaituo Huang, Li Cui, Jing Meng, Jiyan Liang. *J. Electroanal. Chem*., 2018, 817, 202-209.

[11] M. Chen, J. Bi, X. Huang, T. Wang, Z. Wang and H. Hao, *Chemosphere.*, 2021, 278, 130386.

[12] R. Jia, Y. Wang, C. Wang, Y. Ling, Y. Yu and B. Zhang, *ACS Catal*., 2020, 10, 3533-3540.

[13] Y. Yu, C. Wang, Y. Yu, Y. Wang and B. Zhang, Sci. *China Chem*., 2020, 63, 1469-1476.

[14] A. Wei, J. Ma, J. Chen, Y. Zhang, J. Song and X. Yu, *Chem. Eng. J*., 2018, 353, 595-605.

[15] Z.-Y. Wu, M. Karamad, X. Yong, Q. Huang, D. A. Cullen, P. Zhu, C. Xia, Q. Xiao, M. Shakouri, F.-Y. Chen, J. Y. Kim, Y. Xia, K. Heck, Y. Hu, M. S. Wong, Q. Li, I. Gates, S. *Siahrostami and H. Wang, Nat. Commun*., 2021, 12, 2870.

[16] Y. M. Zhang, Y. L. Zhao, Z. Chen, L. Q. Wang, L. C. Zhou, P. P. Wu, F. Wang, and P. Ou. *J. Electrochem. Soc*., 2018, 165, E420-E428.

[17] Y. Wang, Y. Yu, R. Jia, C. Zhang and B. Zhang, *Natl. Sci. Rev*., 2019, 6, 730-738.

[18] W. Teng, J. Fan and W.-x. Zhang, *ACS Appl. Mater. Interfaces*., 2020, 12, 28091-28099.

[19] J. F. Su, W.-F. Kuan, H. Liu and C. P. Huang, *Appl. Catal. B: Environ*., 2019, 257, 117909.

[20] J. Gao, B. Jiang, C. Ni, Y. Qi, Y. Zhang, N. Oturan and M. A. Oturan, *Appl. Catal. B: Environ*., 2019, 254, 391-402.

[21] C. H. Wang, W. Zhou, Z. J. Sun, Y. T. Wang, B. Zhang and Y. F. Yu, *J. Mater. Chem. A*, 2021, *9, 239-243.*

[22] David Reyter, Gwenaël Chamoulaud, Daniel Bélanger, Lionel Roué. J. *Electroanal. Chem*., 2006, 596, 13-24.

[23] Z. Q. Zhang, Y. P. Xu, W. X. Shi, W. Wang, R. J. Zhang, X. Bao, B. Zhang, L. Li, F. Y. Cui. *Chem. Eng. J*., 2016, 290, 201-208.

[24] Y. Guo, R. Zhang, S. C. Zhang, Y. W. Zhao, Q. Yang, Z. D. Huang, B. B. Dong and C. Y. Zhi. *Energy Environ. Sci*., 2021, 14, 3938–3944.
[25] J. Li, G. Zhan, J. Yang, F. Quan, C. Mao, Y. Liu, B. Wang, F. Lei, L. Li, A. W. M. Chan, L. Xu, Y.Shi, Y. Du, W. Hao, P. K. Wong, J. Wang, S.-X. Dou, L. Zhang and J. C. Yu, *J. Am. Chem. Soc*., 2020, 142, 7036-7046.
[26] Z. A. Jonoush, A. Rezaee and A. Ghaffarinejad, *J. Clean. Prod*., 2020, 242, 118569.